

Magnetic Field Simulation of an Induction Motor Using Nonlinear Time-Stepping Finite Element Method

P. Pao-la-or^{*}, S. Peaiyoung^{**}, T. Kulworawanichpong^{*}, and S. Sujitjorn^{*}

^{*} School of Electrical Engineering, Suranaree University of Technology, Thailand, E-mail: padej@ccs.sut.ac.th

^{**} RTAF Academy, Air Education and Training Command, Thailand, E-mail: sompoth1834@yahoo.com

ABSTRACT

This paper presents a mathematical model of magnetic fields in an induction motor. A two-dimensional nonlinear time-stepping finite element method (FEM) is used for the electromagnetic field analysis in an induction machine operating with full load steady-state rotor movement. To solve this time-dependent system, a step-by-step numerical integration of the backward difference algorithm is applied. In addition, the Newton-Raphson (N-R) method is employed to handle the nonlinearities of the system equation. To evaluate its use, a three-phase, four-pole 5-hp squirrel-cage induction motor with double layer winding was tested. As a result, the magnetic flux distribution through the cross-sectional area of the induction motor was well described, graphically, using the flux line plot. Moreover, space and time electromagnetic forces resulting from the magnetic flux were also analyzed.

Keywords: Induction motors, Finite element method, Magnetic field, Time stepping method

1. INTRODUCTION

To design induction machines requires accurate prediction of the machine behaviours, e.g. magnetic flux density, electromagnetic force, etc. These are based on magnetic flux distribution passing the motor cross-sectional area. To analyze magneto-dynamic of the motor, there are two main methods of magnetic flux calculation: i) permeance wave theory and ii) numerical approximation methods (e.g. finite difference: FD or finite element methods: FEM) [1]. With lack of accuracy, the first approach is not often used for this purpose, especially when nonlinearity of magnetic cores is involved. The FEM is applicable to a broad range of solving electromagnetic problems due to its flexibility, and accuracy. Application of the FEM to analyse induction motors is inclusive. In this paper, a time-dependent and a highly saturated field in an induction motor is used for test. The time dependence of the field and the motion of the rotor are modeled by the backward-difference scheme. This results in a set of nonlinear partial differential equations (PDE). Due to its quadratic convergence characteristics, the Newton-Raphson (N-R) method is employed to solve those nonlinear FEM equations.

This paper consists of 4 sections. Section 2 presents the mathematical model of magnetic fields in induction motors based on a set of Maxwell's equations, while Section 3 describes the FEM applied to induction motors for the purpose of obtaining magnetic flux distribution and electromagnetic force wave. Information of the test example and simulation results are shown in Section 4. Finally, the last section provides the conclusion.

2. MODELING OF MAGNETIC FIELD IN INDUCTION MOTORS

To develop the mathematical model of magnetic vector potential \mathbf{A} in a three-phase induction motor, it is assumed that the magnetic field lies in the cross-sectional (x, y) plane. Hence, only the z -component of induced currents can be considered. It also assumes that magnetic material of the motor cores is non-linearly isotropic. Due to the low operating frequency of the supply source (50 Hz), displacement currents are neglected [1]. The fundamental equation describing the space and time variation of the magnetic vector potential \mathbf{A} over the region of analysis which coincides with its component A_z has the following form [2],

$$\frac{\partial}{\partial x} \left(\frac{1}{\mu} \frac{\partial \mathbf{A}}{\partial x} \right) + \frac{\partial}{\partial y} \left(\frac{1}{\mu} \frac{\partial \mathbf{A}}{\partial y} \right) - s \sigma \left(\frac{\partial \mathbf{A}}{\partial t} \right) = J_0 \quad (1)$$

where μ is the permeability of the ferromagnetic material, σ is the conductivity of the conducting media in the rotor, s is the slip at a specific operating condition of the rotor, and J_0 is the applied current density. Although the mathematical modeling of magnetic fields in the induction motors can be expressed in the form of partial differential equations, it is very difficult to determine their exact solution. Frequently, such a problem is analyzed by applying other indirect methods, e.g. FD, FEM, boundary element method (BEM), Method of Moments, etc, which can avoid tedious and complicated computation. In this paper, only the FEM is employed for this approximation.

3. NONLINEAR TIME-STEPPING FEM FOR INDUCTION MOTORS

3.1 Discretization and Rotation

Linear triangular elements are used for discretizing cross-sectional area of the induction motor such that the meshes' coordinates during computing process can be accessed rapidly. In this approach, the FEM meshes of the cross section of the motor are divided into two parts, which are the stator and the rotor, each including a part of the air gap. Meshes of the two parts are generated separately. The air gap is divided into two layers, one of which is to the rotor, and the other is to the stator. When the rotor rotates, the shape of rotor meshes is not changed. Meshes are rotated together with the rotation of the rotor. So only the co-ordinates (x,y) and the periodic boundary conditions of the rotor part are needed to be re-defined. This means that the stator and the rotor meshes are generated once at the beginning and then can be used without any change throughout the computing. A two-dimensional Cartesian-coordinate area is modeled with 6,100 elements and 3,108 nodes to represent the entire motor cross-section. For example, one quarter of the discretized cross-section is depicted in Fig. 1.

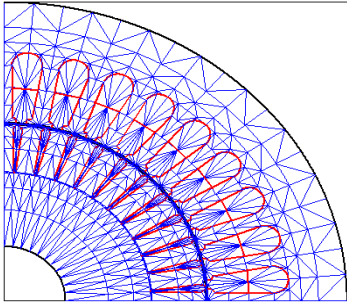


Fig.1: Discretization of the Induction Motor

3.2 Finite Element Formulation

An equation governing each element is derived from the Maxwell's equations directly by using Galerkin approach, which is the particular weighted residual method for which the weighting functions are the same as the shape functions [3]. According to the method, the magnetic vector potential is expressed as

$$A(x, y) = A_i N_i + A_j N_j + A_k N_k \quad (2)$$

where N_n , $n = i, j, k$ is the element shape function and the A_n , $n = i, j, k$ is the approximation of the magnetic vector potential at each node (i, j, k) of the elements, which is

$$N_n = \frac{a_n + b_n x + c_n y}{2\Delta_e} \quad (3)$$

where Δ_e is the area of the triangular element and,

$$\begin{aligned} a_i &= x_j y_k - x_k y_j, & b_i &= y_j - y_k, & c_i &= x_k - x_j \\ a_j &= x_k y_i - x_i y_k, & b_j &= y_k - y_i, & c_j &= x_i - x_k \\ a_k &= x_i y_j - x_j y_i, & b_k &= y_i - y_j, & c_k &= x_j - x_i. \end{aligned}$$

The method of the weighted residual with Galerkin approach is then applied to the differential equation, Eq.(1), where the integrations are performed over the element domain Ω .

$$\begin{aligned} \int_{\Omega} N_n \left(\frac{\partial}{\partial x} \left(\frac{1}{\mu} \frac{\partial \mathbf{A}}{\partial x} \right) + \frac{\partial}{\partial y} \left(\frac{1}{\mu} \frac{\partial \mathbf{A}}{\partial y} \right) \right) d\Omega \\ - \int_{\Omega} N_n s \sigma \left(\frac{\partial \mathbf{A}}{\partial t} \right) d\Omega + \int_{\Omega} (N_n J_0) d\Omega = 0 \end{aligned} \quad (4)$$

or in the compact matrix form

$$[M] \{\dot{A}\} + [K] \{A\} = \{F\} \quad (5)$$

$$[M] = s \sigma \int_{\Omega} N_n N_m d\Omega = \frac{s \sigma \Delta_e}{12} \begin{bmatrix} 2 & 1 & 1 \\ 1 & 2 & 1 \\ 1 & 1 & 2 \end{bmatrix}$$

$$\begin{aligned} [K] &= \nu \int_{\Omega} \left(\frac{\partial N_n}{\partial x} \frac{\partial N_m}{\partial x} + \frac{\partial N_n}{\partial y} \frac{\partial N_m}{\partial y} \right) d\Omega \\ &= \frac{\nu}{4\Delta_e} \begin{bmatrix} b_i b_i + c_i c_i & b_i b_j + c_i c_j & b_i b_k + c_i c_k \\ & b_j b_j + c_j c_j & b_j b_k + c_j c_k \\ & & b_k b_k + c_k c_k \end{bmatrix} \\ &= \frac{\nu}{4\Delta_e} \begin{bmatrix} S_{ii} & S_{ij} & S_{ik} \\ S_{ji} & S_{jj} & S_{jk} \\ S_{ki} & S_{kj} & S_{kk} \end{bmatrix} \end{aligned}$$

$$\{F\} = J_0 \int_{\Omega} N_n d\Omega = \frac{\Delta_e}{3} \begin{bmatrix} J_0 \\ J_0 \\ J_0 \end{bmatrix}$$

where ν is the reluctivity of material ($\nu = 1/\mu$).

3.3 Equation Arising from the Time-Stepping FEM

The method of discretization used herein is based on Eq.(6). Therefore, a time-dependent field is solved by discretizing the time at short time interval Δt . Although there are three basic methods of the time discretization: forward difference method ($\beta=0$), backward difference method ($\beta=1$), and Crank-Nicholson method ($\beta=1/2$), the backward difference is used due to its convergence [4].

$$\beta \{A\}^{t+\Delta t} + (1-\beta) \{A\}^t = \frac{\{A\}^{t+\Delta t} - \{A\}^t}{\Delta t} \quad (6)$$

For this technique, Eq.(5) can be rewritten at time $t+\Delta t$. Thus, Eq.(5) becomes Eq.(7). Insert Eq.(6) into Eq.(7), Eq.(8) can be obtained.

$$[M] \{\dot{A}\}^{t+\Delta t} + [K] \{A\}^{t+\Delta t} = \{F\}^{t+\Delta t} \quad (7)$$

$$\left(\frac{1}{\Delta t} [M] + [K] \right) \{A\}^{t+\Delta t} = \frac{1}{\Delta t} [M] \{A\}^t + \{F\}^{t+\Delta t} \quad (8)$$

3.4 N-R Method for Nonlinear FEM Problems

This problem is intrinsically nonlinear due to the presence of ferromagnetic materials. Therefore, the well-known N-R method is employed to handle this nonlinearity. The permeability is $\mu_0 = 4\pi \times 10^{-10}$ H/mm in nonmagnetic regions. In the stator and rotor cores, the permeability is determined by the absolute value of the flux density, \mathbf{B} , referring to a magnetization curve stored for a look-up table. Magnetic saturation can be taken into account by the use of the B - H curve. Extraction of the data along the curve herein uses cubic spline interpolation. For all points beyond the range of available data, the curve can be linearly extrapolated.

To formulate the problem, all the equations governing each element similar to Eq.(8) are collected to form the system matrix. Let G represent the first row of Eq.(8), thus Eq.(9) is found.

$$G = \frac{s\sigma\Delta_e}{12\Delta t} (2A_i^{t+\Delta t} + A_j^{t+\Delta t} + A_k^{t+\Delta t}) + \frac{v^{t+\Delta t}}{4\Delta_e} (S_{ii}A_i^{t+\Delta t} + S_{ij}A_j^{t+\Delta t} + S_{ik}A_k^{t+\Delta t}) - \frac{s\sigma\Delta_e}{12\Delta t} (2A_i^t + A_j^t + A_k^t) - \frac{J_0^{t+\Delta t}\Delta_e}{3} \quad (9)$$

The N-R method requires the first partial derivatives of G with respect to the nodal magnetic vector potentials of A_i , A_j and A_k . For example, only the derivative of G with respect to A_i is shown as follows,

$$\frac{\partial G}{\partial A_i^{t+\Delta t}} = \frac{2s\sigma\Delta_e}{12\Delta t} + \frac{v^{t+\Delta t}}{4\Delta_e} S_{ii} + \frac{1}{4\Delta_e} (S_{ii}A_i^{t+\Delta t} + S_{ij}A_j^{t+\Delta t} + S_{ik}A_k^{t+\Delta t}) \left(\frac{\partial v}{\partial B^2} \right)^{t+\Delta t} \left(\frac{\partial B^2}{\partial A_i} \right)^{t+\Delta t}$$

Once the chain rule is applied, $\frac{\partial v}{\partial A}$ can be replaced by

$\frac{\partial v}{\partial B^2} \frac{\partial B^2}{\partial A}$ [5], where $\frac{\partial v}{\partial B^2}$ is obtained from the v - B^2 curve. For the N-R method, the first-row equation of the element, of which i, j and k are vertexes, is

$$\frac{\partial G}{\partial A_i^{t+\Delta t}} \Delta A_i^{t+\Delta t} + \frac{\partial G}{\partial A_j^{t+\Delta t}} \Delta A_j^{t+\Delta t} + \frac{\partial G}{\partial A_k^{t+\Delta t}} \Delta A_k^{t+\Delta t} = -G$$

where $\Delta A_i^{t+\Delta t} = A_{m+1}^{t+\Delta t} - A_m^{t+\Delta t}$ and m is the iteration number of the N-R method. In the similar manner, with H and I being the second and the third row equations, respectively, the matrix form of the N-R equation governing this element can be found as Eq.(10), where the first matrix of Eq.(10) is the Jacobian matrix.

$$\begin{bmatrix} \frac{\partial G}{\partial A_i^{t+\Delta t}} & \frac{\partial G}{\partial A_j^{t+\Delta t}} & \frac{\partial G}{\partial A_k^{t+\Delta t}} \\ \frac{\partial H}{\partial A_i^{t+\Delta t}} & \frac{\partial H}{\partial A_j^{t+\Delta t}} & \frac{\partial H}{\partial A_k^{t+\Delta t}} \\ \frac{\partial I}{\partial A_i^{t+\Delta t}} & \frac{\partial I}{\partial A_j^{t+\Delta t}} & \frac{\partial I}{\partial A_k^{t+\Delta t}} \end{bmatrix} \begin{bmatrix} \Delta A_i^{t+\Delta t} \\ \Delta A_j^{t+\Delta t} \\ \Delta A_k^{t+\Delta t} \end{bmatrix} = - \begin{bmatrix} G \\ H \\ I \end{bmatrix} \quad (10)$$

For one element containing 3 nodes, the expression of the N-R approximation is a 3×3 matrix. With the account of all elements in the system of n nodes, the system equation is sizable as an $n \times n$ matrix.

4. SIMULATION AND RESULTS

The boundary conditions applied here are zero magnetic vector potentials at the outer perimeter of the stator core and the inner perimeter of the rotor core. In addition, the banded diagonal matrix storage together with the bi-conjugate gradient method (BCGM) for solving a set of linear equations is used to speed up the computation. In time-stepping FEM, the information from the last step can be successfully used to reduce the computing time when solving the current FEM equations. The machine used in this paper is a three-phase, four-pole, Y-connected, 5-hp squirrel cage induction motor with a double layer winding of 7/9 pitch coil. The motor is fed by a 380-V, 50-Hz sinusoidal source at full load (slip=0.03). The motor possesses 36 stator slots and 44 unskewed rotor slots. Also, current flowing through a coil in each slot is assumed to distribute sinusoidally and can be simply obtained from the well-known equivalent circuit of induction motors.

The test system previously described is simulated by an FEM solver written in C. The simulation are performed in a 1.6 GHz, 512-MB SD-RAM Pentium IV computer. Due to the steady-state operation, the simulated time step ($\Delta t = 0.1145$ ms for $\Delta\theta = 1^\circ$ of the rotor movement) is uniform. The computational time for each simulated time step is approximately 5 minutes. It notes that error tolerance of the N-R method and the BCGM is 1×10^{-9} and 1×10^{-15} , respectively. Numerical results of the magnetic flux obtained are illustrated as shown in Figs 2a) – 2d) using MATLAB™. Figs 2a) – 2d) illustrate the flux distribution of the motor cross-section (in Wb/mm) at full load resulting from the change of rotor position of 0, 30, 60 and 90 degrees counter-clockwise, respectively. As a result, there are four regions of magnetic flux lines circulating the slot with the highest current density, so-called the magnetic pole. This explains that permeance of the magnetic path of the regions around the magnetic pole is low. Interestingly, the movement of the flux line plot in these four rotor positions also show the magnetic fields revolving in counter-clockwise direction.

In addition, the curl of the magnetic vector potential \mathbf{A} is magnetic flux density \mathbf{B} ($\mathbf{B} = \nabla \times \mathbf{A}$). Its components along x and y axes are computed by

$$B_x = \frac{\partial A_z}{\partial y} = \frac{c_i A_i + c_j A_j + c_k A_k}{2\Delta_e} \quad (11)$$

$$B_y = -\frac{\partial A_z}{\partial x} = -\left(\frac{b_i A_i + b_j A_j + b_k A_k}{2\Delta_e}\right) \quad (12)$$

Moreover, radial flux density B_r and tangential flux density B_t acting on the air-gap can be expressed in cylindrical coordinate as a function of B_x and B_y , i.e.

$$B_r = B_x \cos \phi + B_y \sin \phi, B_t = -B_x \sin \phi + B_y \cos \phi$$

where ϕ is the counter-clockwise angle of a stator-tooth center with respect to the positively horizontal axis. The first stator tooth is assigned to the tooth between the slots 1 and 36.

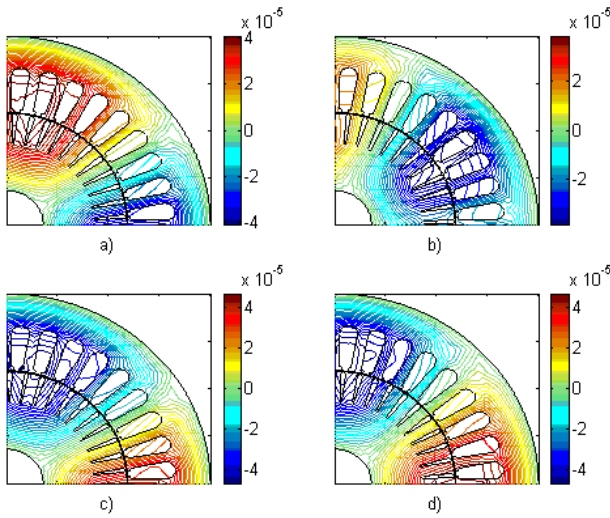


Fig.2: Flux Line Plot at each Position
a) 0°: b) 30°: c) 60°: d) 90°

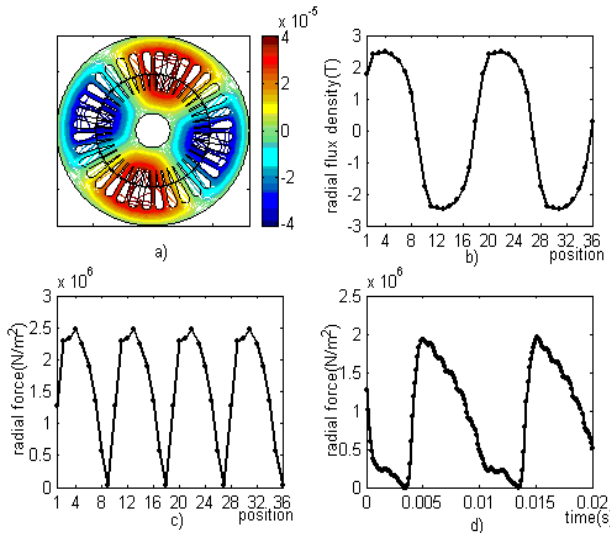


Fig.3: a) Flux Line Plot, b) Space Flux Density Wave,
c) Space Electromagnetic Force Wave,
d) Time Electromagnetic Force Wave

The magnetic flux density acting on the air gap in the radial direction can be depicted as shown in Fig. 3b)

which corresponds to Fig. 3a). As can be seen, the curve in Fig. 3b) resembles to sinusoid. The waveform is apparently distorted due to the non-linearity of the magnetic material. The peak values of the magnetic flux density appear at the stator teeth 4, 13, 22 and 31, which correspond to zero magnetic vector potential. Whilst, the magnetic flux densities of the stator teeth 9, 18, 27 and 36 are approximately zero, and their corresponding magnetic vector potentials are peaks. Maxwell's stress equations were also used to determine the distribution of the electromagnetic forces across the air gap obtained from $F_r = (1/2\mu_0)(B_r^2 - B_t^2)$ [6] and is shown in Fig. 3c). With the time component, flux density waves were calculated at the center of each of the 36 stator teeth for each rotor position over 360°. The results for the centre of the first stator tooth are depicted as shown in Fig. 3d).

5. CONCLUSIONS

This paper describes the modeling and simulation technique of the magnetic flux distribution in induction motors by using the Finite Element Method (FEM). The results show that this method is simple and effective to illustrate how magnetic flux passing through the motor cross-section. With this advantage, further work based on magnetic flux calculation to analyze the induction motors, e.g. magnetic vibration, noise, harmonic, heat losses, etc. can be developed and, with this simplification, difficulty of computing is considerably reduced or eliminated.

6. REFERENCES

- [1] N. A. Demerdash, and D. H. Gillott, "A new approach for determination of eddy current and flux penetration in nonlinear ferromagnetic materials," *IEEE Transactions on Magnetics*, Vol. 74, pp. 682-685, 1974.
- [2] E. Vassent, G. Meunier, and A. Foggia, "Simulation of induction machines-using complex magnetodynamic finite element method coupled with the circuit equations," *IEEE Transactions on Magnetics*, Vol. 27, No. 5, pp. 4246-4249, 1991.
- [3] T. W. Preston, A. B. J. Reece, and P. S. Sangha, "Induction motor analysis by time-stepping techniques," *IEEE Transactions on Magnetics*, Vol. 24, No. 1, pp. 471-474, 1988.
- [4] M.A. Jabbar, H.N. Phyu, Z.J. Liu, and C. Bi, "Modeling and numerical simulation of a brushless permanent-magnet dc motor in dynamic conditions by time-stepping technique," *IEEE Transactions on Industrial Applications*, Vol. 40, No. 3, pp. 763-769, 2004.
- [5] S. J. Salon, *Finite element analysis of electrical machines*, Kluwer Academic Publishers, USA, 1995.
- [6] S. Sakamoto, T. Hirata, T. Kobayashi, and K. Kajiwara, "Vibration analysis considering higher harmonics of electromagnetic forces for rotating electric machines," *IEEE Transaction on Magnetic*, Vol. 35, No. 3, pp. 1662-1665, 1999.